AIP | Journal of Applied Physics

Linear axial scattering of an acoustical high-order Bessel trigonometric beam by compressible soft fluid spheres

F. G. Mitri

Citation: J. Appl. Phys. **109**, 014916 (2011); doi: 10.1063/1.3518496
View online: http://dx.doi.org/10.1063/1.3518496
View Table of Contents: http://jap.aip.org/resource/1/JAPIAU/v109/i1
Published by the American Institute of Physics.

Linear axial scattering of an acoustical high-order Bessel trigonometric beam by compressible soft fluid spheres

F. G. Mitri[a)]
Los Alamos National Laboratory, MPA-11, Sensors and Electrochemical Devices, Acoustics and Sensors Technology Team, MS D429, Los Alamos, New Mexico 87545, USA

(Received 22 June 2010; accepted 20 October 2010; published online 14 January 2011)

The acoustic scattering properties of nondiffracting high-order Bessel trigonometric beams (HOBTBs) by fluid spheres are investigated. The three-dimensional directivity acoustic scattering patterns of hexane, red blood, and mercury soft spheres immersed in water and centered on the beam axis of wave propagation are presented and discussed. HOBTBs belong to the family of nondiffracting beams and are proper solutions of the homogeneous (source-free) Helmholtz equation. Closed-form analytical solutions for the incident and scattered pressure fields are provided. The far-field acoustic scattering field is expressed as a partial wave series involving the scattering angle relative to the beam axis, the order, and the half-conical angle of the wave number components of the HOBTB. The properties of the acoustic scattering by fluid spheres are discussed and numerical computations with animated graphics show exciting scattering phenomena that are especially useful in applications related to particle entrapment and manipulation of soft matter using acoustic HOBTBs. Other potential applications may include medical or nondestructive ultrasound imaging with contrast agents, or monitoring of the manufacturing processes of sample soft matter systems with HOBTBs. © *2011 American Institute of Physics*. [doi:10.1063/1.3518496]

I. INTRODUCTION

Increasing interest in the properties of acoustic wave scattering by particles drives innovation in various applications including sensor/sonar design,[1–3] medical imaging with contrast agents,[4–6] and metamaterials[7–11] to name a few relevant areas. The scattering mechanisms, during which the incident wave field deviates from its original path because of the presence of the scatterer, depend generally on the viscoelastic properties of the target as well as the characteristics of the incident beam. Appropriate selection of the beam's parameters, such as the focus, waist, divergence, directionality, collimation, etc., or more generally the beam's type [i.e., diffracting, (i.e., Gaussian, Bessel–Gaussian, Laguerre–Gaussian, fractional Bessel, etc.) versus nondiffracting, (i.e., Bessel of integer order, high-order Bessel Beam of fractional type α, etc.)], may be used to advantage to enhance or suppress the scattering.[12–17]

Ideal nondiffracting beams are proper solutions of the homogeneous (source-free) Helmholtz equation,[18] for which the transverse pressure (or intensity) distribution profile remains unchanged during wave propagation. In practice, a very close approximation to an ideal nondiffracting beam can be achieved experimentally by a Gaussian transmittance apodization to produce a "limited-diffracting"-Gauss beam. Such a procedure has been successfully used to produce practical optical Bessel–Gauss[19–23] and high-order Bessel–Gauss beams of fractional type α.[24]

The purpose of this research is to investigate the axial acoustic scattering properties of a nondiffracting high-order Bessel beam incident upon a spherical target (Fig. 1), and having an azimuthal dependency in the form of $\cos(|m|\phi \pm \phi_0)$, where m is referred to as the order of the beam or the topological charge. Because of the phase dependency on the cosine function, this family of Bessel beams is termed here as a *high-order Bessel trigonometric beam* (HOBTB) to avoid a possible confusion with the terminology high-order Bessel *vortex* (or helicoidal) beam.[13–15] A vortex beam has an azimuthal dependency described mathematically by the exponential $e^{i|m|\phi}$, where m can be any positive or negative integer. This type of vortex beams has a phase ramp equal to the azimuthal angle. On the other hand, the corresponding distribution of the pressure magnitude and phase in space of a HOBTB is fundamentally different from a vortex beam as shown by comparing Fig. 2 here with Fig. 1 of Ref. 13.

In this investigation, closed-form solutions for the total acoustic scattering field of a HOBTB by compressible soft fluid spheres immersed in an ideal fluid and centered along the axis of the incident beam are derived. Predictions

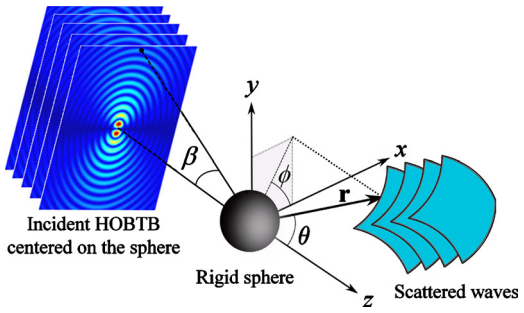

FIG. 1. (Color online) Geometry of the problem. A rigid immovable sphere is placed along the z-axis of a HOBTB of progressive waves (in this figure, a first-order Bessel trigonometric beam). The plane-wave fronts constructing the beam have a half-cone angle β with respect to the z-axis, and θ and ϕ are the polar and azimuthal angles, respectively.

[a)]Electronic addresses: mitri@lanl.gov and mitri@ieee.org.

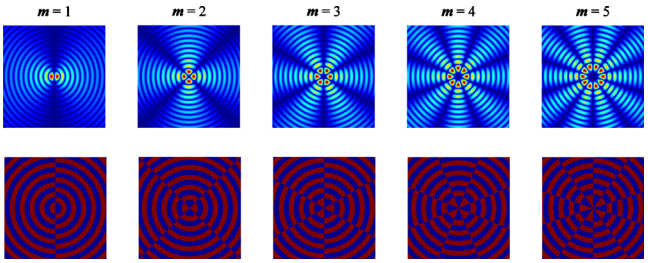

FIG. 2. (Color online) Theoretical moduli (upper row) and phases (inferior row) cross-sections of Bessel trigonometric beams of order $m=1$ to 5, respectively. Physically, the plots determine the magnitudes and phases of the incident acoustic pressure field distribution in space. The transverse wave number used for the simulations is $k_r=6.5\times10^4$ m^{-1}, and the spatial $R=\sqrt{(x^2+y^2)}$ where -1.15 mm$\leq x, y\leq 1.15$ mm. The polar angle of position in the plane is varied from $0\leq\phi=\tan^{-1}(y/x)\leq 2\pi$ with an initial (arbitrary) phase $\phi_0=0$ chosen as an example.

through numerical analyses are evaluated and some properties of the scattering are examined and discussed. The fluid particles having spherical geometries are approximations of first order to attempt at building a realistic model predicting the behavior of acoustically-interacting organelles and cells in a large number of biophysical and biomedical applications. The examples provided herein are relevant for potential applications in the field of soft matter physical acoustics, particularly from the standpoint of both the acoustic scattering and acoustic radiation force in related particle manipulation of biological/chemical materials, as well as in other areas of research in medical or nondestructive ultrasound imaging with contrast agents, or monitoring of the manufacturing processes of sample soft matter systems.

II. THEORETICAL ANALYSIS OF THE ACOUSTIC SCATTERING OF A HOBTB BY A FLUID SPHERE

Using the analogy with the electromagnetic field representation of a cylindrical wave function [(80) p. 412 in Ref. 25], the incident acoustic (complex) pressure produced by a nondiffracting HOBTB is expressed as

$$P^{(inc)}_{\mathrm{HOBTB}}(r,\theta,\phi,t) = P_0(i^{-|m|}/2\pi)\int_0^{2\pi} e^{i(\mathbf{k}\cdot\mathbf{r}-\omega t)}\cos(|m|\phi'\pm\phi_0)d\phi', \qquad (1)$$

where P_0 is the pressure amplitude, the components of $\mathbf{r}$ in spherical coordinates are $(r\sin\theta\cos\phi, r\sin\theta\sin\phi, r\cos\theta)$ (see Fig. 1), and the components of the wave-vector $\mathbf{k}$ are $(k\sin\beta\cos\phi', k\sin\beta\sin\phi', k\cos\beta)$, the parameter $k=\omega/c=2\pi/\lambda$, is defined as the wave-number of the incident HOBTB, ω is the angular frequency, c is the speed of sound in the fluid medium, λ being the wavelength of the acoustic radiation making up the beam, β is the half-cone angle formed by the wave-vector $\mathbf{k}$ relative to the axis of wave propagation, r, θ, ϕ, are the radial, polar, and azimuthal components respectively, ϕ' is the azimuthal angle of the individual plane-wave components of the beam, and ϕ_0 is an initial arbitrary azimuthal (phase) angle.

Equation (1) shows that the HOBTB is constructed by means of a superposition of plane waves propagating over a cone with half-angle β, and expressed mathematically by the integration over the differential azimuthal angle $d\phi'$. This approach was used to model the electromagnetic[26,27] and acoustic[12] field of a zero-order Bessel beam as well as in the description of an acoustical Bessel *vortex* beam of unit topological charge[14] that is a particular case of a generalized solution given initially in Refs. 13, 15, and 25.

After performing the integration in (1) and manipulating the result using [(57) p. 409 in Ref. 25], it follows that the incident pressure field is expressed as

$$\begin{aligned} P^{(inc)}_{\mathrm{HOBTB}}(r,\theta,\phi,t) &= P_0 e^{i(kr\cos\beta\cos\theta-\omega t)} \\ &\times J_{|m|}(kr\sin\beta\sin\theta)\cos(|m|\phi\pm\phi_0), \\ &= P_0 e^{-i\omega t}\sum_{n=|m|}^{\infty}\frac{(n-|m|)!}{(n+|m|)!}(2n+1) \\ &\times i^{(n-|m|)}j_n(kr)P_n^{|m|}(\cos\theta) \\ &\times P_n^{|m|}(\cos\beta)\cos(|m|\phi\pm\phi_0), \end{aligned} \qquad (2)$$

consistent with [(82) p. 413 in Ref. 25].

Equation (2) describes the pressure of a HOBTB incident upon a sphere, whose center is located at a distance r from an observation point, $j_n(.)$ is the spherical Bessel function of the first kind of order n, $P_n^m(.)$ are the associated Legendre functions, and θ is the scattering (polar) angle relative to the beam axis of wave propagation z.

It is important to note that (1) and (2) are proper solutions of the Helmholtz wave equation. With $\phi_0=m=0$, (2) reduces to the expression of a zero-order Bessel beam.[12]

The (complex) pressure field scattered by a spherical object placed along the axis of wave propagation of a HOBTB is expressed as

$$\begin{aligned} P^{(sc)}_{\mathrm{HOBTB}}(r,\theta,\phi,t) &= P_0 e^{-i\omega t}\sum_{n=|m|}^{\infty}\frac{(n-|m|)!}{(n+|m|)!}(2n+1) \\ &\times i^{(n-|m|)}h_n^{(1)}(kr)S_n P_n^{|m|}(\cos\theta) \\ &\times P_n^{|m|}(\cos\beta)\cos(|m|\phi\pm\phi_0). \end{aligned} \qquad (3)$$

Equation (3) describes the scattered field in the near-field region ($r\geq a$) where a is the sphere's radius. It is, however, common in applications such as medical/nondestructive ultrasound and sonar imaging to measure the far-field scattered pressure. In the far-field region ($r\gg a$), the spherical Hankel function of the first kind $h_n^{(1)}(\cdot)$ reduces to the following asymptotic approximation; $h_n^{(1)}(kr)\underset{kr\to\infty}{\rightarrow}(1/i^{(n+1)}kr)e^{ikr}$. Therefore, the steady-state (time-independent) scattered pressure in the far-field from a sphere[28,29] is expressed as

$$P^{(sc)}_{\mathrm{HOBTB}}(r,\theta,\phi)\underset{kr\to\infty}{=}P_0\frac{a}{2r}f^{(m)}_{\mathrm{HOBTB},\infty}e^{ikr}, \qquad (4)$$

where the (complex) form function for a sphere is defined by the partial wave series as

$$f^{(m)}_{\mathrm{HOBTB},\infty}(ka,\theta,\phi)=\frac{2}{ika}\sum_{n=|m|}^{\infty}\frac{(n-|m|)!}{(n+|m|)!}(2n+1)\times i^{(-|m|)}S_nP_n^{|m|}(\cos\theta)\times P_n^{|m|}(\cos\beta)\cos(|m|\phi\pm\phi_0). \quad (5)$$

Equation (5) represents the total form function for a HOBTB scattered by a sphere. For a fluid sphere, the scattering coefficients S_n are obtained from the boundary conditions at the interface between the fluid sphere and its surrounding fluid medium. At this interface, the radial displacements (or velocities) and normal stresses must be continuous leading to the following form for the coefficients S_n as follows:

$$S_n=\frac{\det\begin{bmatrix}\gamma j_n(ka) & j_n(k_{fs}a)\\ j_n'(ka) & j_n'(k_{fs}a)\end{bmatrix}}{\det\begin{bmatrix}-\gamma h_n^{(1)}(ka) & j_n(k_{fs}a)\\ -h_n^{(1)}(ka) & j_n'(k_{fs}a)\end{bmatrix}}, \quad (6)$$

where $\gamma=(\rho c/\rho_{fs}c_{fs})$, ρ_{fs}, and c_{fs} are the density and speed of sound inside the fluid sphere.

For an infinitely soft sphere, $\rho_{fs}\to 0$, and hence, the sphere possesses no inertia. The coefficients S_n reduce to,

$$S_n=S_n^s=-j_n(ka)/h_n^{(1)}(ka), \quad (7)$$

where S_n^s are known as the scattering coefficients for an infinitely soft sphere.

III. NUMERICAL EXAMPLES AND DISCUSSION

Realizing the number of variables in (5), the main attempt made here is to study the variations in the magnitude of the total form function versus the order m of the HOBTB. A MATLAB® code is constructed for computing the scattering coefficients (6) and plotting the magnitude of the total (far-field) scattering form function for the fluid soft spheres given by (5), though the near-field scattering can be predicted using (3) at any distance r from the center of the sphere. However, only the far-field scattering is investigated here as an example to illustrate the theory. In the following calculations, the surrounding fluid is assumed to be nonviscous water with its assumed properties for density $\rho_{\mathrm{water}}=1000$ kg/m^3 and sound speed $c_{\mathrm{water}}=1500$ m/s. Accurate computation of the spherical Bessel and spherical Hankel functions and their derivatives is achieved using modified versions of the specialized math functions "besselj," "bessely," and "besselh" within the software package. The computations are performed on an Intel(R) Core(TM)2 Quad CPU Q9650 @ 3.00 GHz, 3.25 GB of RAM personal computer with a truncation constant largely exceeding ka to ensure proper convergence of the series in (5). The polar and azimuthal angles are varied in the ranges $[0\le\theta\le 2\pi]$, $[-(\pi/2)\le\phi\le(\pi/2)]$ in increments of $\Delta\theta,\Delta\phi=(\pi/100)$, at a selected $ka=5$ and a half-cone angle $\beta=25°$. Because the MATLAB software package uses a Cartesian coordinates system for data display, the "sph2cart" built-in function is employed to properly display the numerical results originally computed using (5) in a spherical coordinates system.

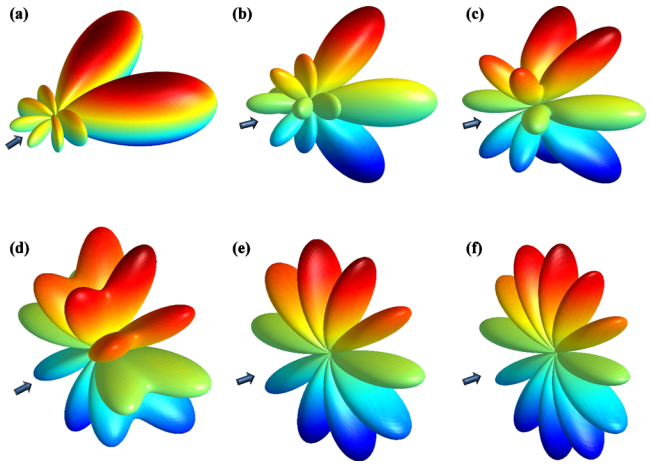

FIG. 3. (Color online) The 3D directivity diagram plots of the scattering form function's modulus as given by (5). The plots are for a fluid hexane sphere in water for $ka=5$, $\beta=25°$, and $\phi_0=0$. The order m of the beam is varied from 1 to 6 corresponding to (a)–(f), respectively. The arrow at the bottom left hand side of each plot indicates the direction of the incident waves.

Consider now the case of fluid spheres placed along the axis of a HOBTB of progressive waves. Three typical examples are chosen here, in which the density of the fluid sphere is smaller (hexane sphere, $\rho_{fs}=656$ kg/m^3, $c_{fs}=1078.5$ m/s), closer [red blood sphere (RBS), $\rho_{fs}=1099$ kg/m^3, $c_{fs}=1631$ m/s], and higher (mercury sphere, $\rho_{fs}=13600$ kg/m^3, $c_{fs}=1407$ m/s) than the density of the surrounding fluid (water), respectively.

Figures 3(a)–3(f) show the predictions of the total scattering form function [i.e., (5)] modulus for a hexane fluid sphere placed in a first-to sixth-order Bessel trigonometric beam, respectively. The plots are computed for a half-cone angle $\beta=25°$ at $ka=5$ and $\phi_0=0$. The arrow on the left hand side of each plot indicates the direction of the incident waves. One clearly notices the difference between the three-dimensional (3D) scattering directivity plots as the order m increases. Moreover, the directivity patterns of the acoustic scattering field are closely related to the shape of the incident beam (see Fig. 2); as the order of the beam increases, additional scattering sound lobes tend to appear.

Figures 4(a)–4(f) show the same predictions as in Figs. 3(a)–3(f) but for a RBS. This particular example is of particular interest in bioengineering applications that aim to study the scattering properties of a red blood cell. In contrast to Figs. 3(a)–3(f), the 3D acoustic scattering directivity patterns of a RBS in Figs. 4(a)–4(f) exhibit quite different behaviors from the hexane sphere; note the appearance of additional sound lobes in the forward hemispherical region for $m=5$ [i.e., Fig. 3(e)]. An additional computation is performed to compute the 3D directivity patterns for a RBS in the field of a second-order Bessel trigonometric beam in the range $4\le ka\le 7$. See supplementary material in Ref. 30 that shows the appearance of additional scattering lobes in the backward hemispherical region as ka increases.

Figures 5(a)–5(f) show the 3D directivity patterns computations of the total scattering form function modulus for a mercury sphere immersed in water, that are quite different from the RBS and hexane sphere results. An additional cal-

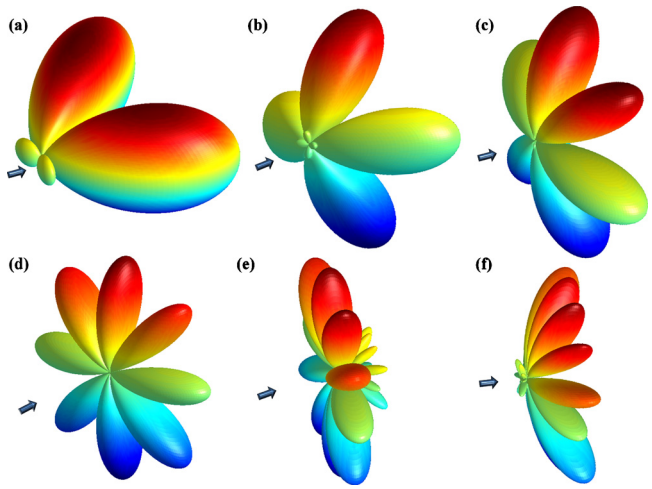

FIG. 4. (Color online) The same as in Fig. 3, however, the plots are for a RBS in water for $ka=5$, $\beta=25°$, and $\phi_0=0$. The order m of the beam is varied from 1 to 6 corresponding to (a)–(f), respectively. See supplementary material in Ref. 30 which corresponds to the 3D acoustic scattering of a second-order Bessel trigonometric beam by a RBS in water in the range $4 \leq ka \leq 7$.

culation is made to study the effect of varying ϕ_0 on the 3D directivity patterns. The 3D acoustic scattering from a mercury sphere in water corresponding to a sixth-order Bessel trigonometric beam [i.e., Fig. 5(f)] is chosen as an example in which the initial arbitrary phase angle ϕ_0 is varied in the range $0 \leq \phi_0 \leq \pi$ repeated 12 times to accommodate a full rotation (i.e., $2m\pi$) in increments of $\delta\phi_0 = \pi/18$. See supplementary material in Ref. 30. As observed from this animation, rotation of the scattering in the azimuthal plane can be achieved by appropriate selection of the initial phase angle. Furthermore, negative values of ϕ_0 can also be selected to rotate the scattering patterns in the opposite sense as shown in the following. The 3D directivity scattering patterns are closely connected to the incident beam. Rotation of the scattering by appropriate selection of ϕ_0 results from rotating the incident beam; additional simulations for the modulus and phase of the incident pressure field of a forth-order Bessel trigonometric beam are performed for which the initial arbitrary phase angle ϕ_0 is varied in the ranges $0 \leq \phi_0 \leq \pi$ and $-\pi \leq \phi_0 \leq 0$, respectively. See supplementary material in Ref. 30. Moreover, one can induce alternate positive and negative values of ϕ_0 so as to create an acoustical switch of the scattering or the incident beam, which may be useful in related acoustic communication applications.

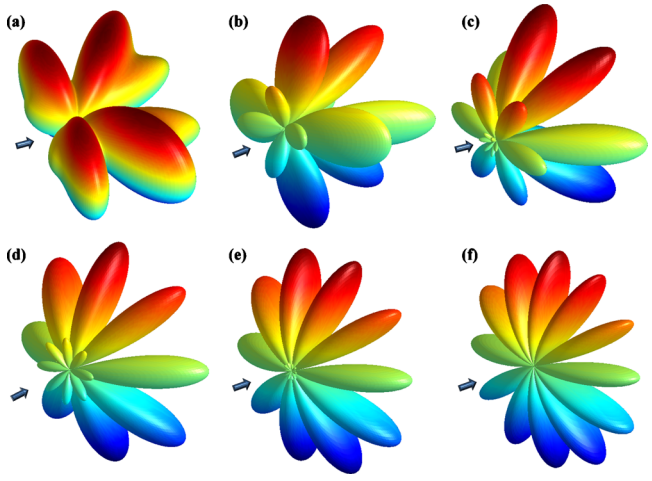

FIG. 5. (Color online) The same as in Fig. 3, however, the plots are for a fluid mercury sphere in water for $ka=5$, $\beta=25°$, and $\phi_0=0$. The order m of the beam is varied from 1 to 6 corresponding to (a)–(f), respectively. Significant differences in the 3D directivity diagram plots occur as compared to Figs. 3 and 4. The effect of varying ϕ_0 on the 3D directivity pattern for the scattering is investigated for a fluid mercury sphere in water placed in the field of a sixth-order Bessel trigonometric beam [i.e., Fig. 5(f)]. See supplementary material in Ref. 30.

Further mathematical analysis of (5) shows the direct dependence on the associated Legendre functions $P_n^{|m|}(\cos\beta)$. Some of the roots of the $P_n^{|m|}(\cos\beta)$ functions were previously evaluated and tabulated in Ref. 31. The specific "root" angles are associated with specific nth partial waves such that the suppression of a particular resonance and its contribution to the scattering is therefore attainable by judicious selection of the half-cone angle β to correspond to on the $P_n^{|m|}(\cos\beta)$ roots. This has been confirmed in the context of the acoustic scattering[13,14,16] and radiation forces[31,32] of Bessel vortex (or helicoidal) beams in suppressing resonances and may be potentially extended to the case of HOBTBs.

The model presented here is valid to predict the 3D acoustic scattering from a single inviscid fluid sphere. Other types may be investigated such as a polymer, protein or lipid spheres providing that their appropriate scattering coefficients are used. For a fluid viscous sphere, absorption within the interior core can be modeled by introducing a complex wave number into the theory $\tilde{k}_{fs}$ such that $\tilde{k}_{fs} = k_{fs}(1 + i\gamma_{fs})$, where γ_{fs} is the normalized absorption coefficient. This technique accounts for systems in which absorption increases linearly with frequency (linear viscoelasticity).

IV. CONCLUSION

The axial acoustic scattering properties of soft fluid spheres along with analytical expressions for the incident and scattered acoustic pressure field of a HOBTB are presented and discussed. The far-field acoustic scattering form function (representing the scattered pressure field is the far-field) is expressed as a partial wave series involving the scattering angle relative to the beam axis, the order, and the half-conical angle of the wave number components of the beam. Numerical computations with animated graphics of the 3D directivity plots show particular properties of the scattering not observed with other conventional beams. Moreover, the sphere's mechanical properties influence the scattering such that additional sound lobes appear in the forward or the backward hemispherical regions. These results are especially useful in entrapment and manipulation applications of soft particles using acoustic HOBTBs.

ACKNOWLEDGMENTS

The author acknowledges the financial support provided through a Director's fellowship (LDRD-X9N9) from Los Alamos National Laboratory. Disclosure: this unclassified

publication, with the following Reference No. LA-UR 10-07253, has been approved for unlimited public release under DUSA ENSCI.

[1]D. M. Deveau and A. P. Lyons, IEEE J. Ocean. Eng. **34**, 93 (2009).
[2]R. Pinkel, M. Merrifield, and H. Ramm, J. Geophys. Res., [Oceans] **100**, 4693 (1995).
[3]J. A. Bucaro, N. Lagakos, B. H. Houston, J. Jarzynski, and M. Zalalutdinov, J. Acoust. Soc. Am. **118**, 1406 (2005).
[4]N. de Jong, A. Bouakaz, and P. Frinking, Echocardiography—J. Cardiovascular Ultrasound and Allied Techniques **19**, 229 (2002).
[5]M. Postema and G. Schmitz, Expert Rev. Mol. Diagn. **6**, 493 (2006).
[6]N. de Jong, A. Bouakaz, and F. J. Ten Cate, Ultrasonics **40**, 567 (2002).
[7]M. Farhat, S. Guenneau, and S. Enoch, Phys. Rev. Lett. **103**, 024301 (2009).
[8]V. Fokin, M. Ambati, C. Sun, and X. Zhang, Phys. Rev. B **76**, 144302 (2007).
[9]D. Torrent and J. Sanchez-Dehesa, New J. Phys. **9**, 323 (2007).
[10]Y. Wu and Z. Q. Zhang, Phys. Rev. B **79**, 195111 (2009).
[11]V. Leroy, A. Strybulevych, M. Scanlon, and J. Page, Eur. Phys. J. E **29**, 123 (2009).
[12]P. L. Marston, J. Acoust. Soc. Am. **121**, 753 (2007).
[13]F. G. Mitri, Ann. Phys. (N.Y.) **323**, 2840 (2008).
[14]P. L. Marston, J. Acoust. Soc. Am. **124**, 2905 (2008).
[15]F. G. Mitri, IEEE Trans. Ultrason. Ferroelectr. Freq. Control **56**, 1100 (2009).
[16]F. G. Mitri, Ultrasonics **50**, 387 (2010).
[17]F. G. Mitri, IEEE Trans. Ultrason. Ferroelectr. Freq. Control **57**, 395 (2010).
[18]J.-Y. Lu, in *Localized Waves*, edited by M. Z.-R. Hugo, E. Hernández-Figueroa, and E. Recami (Wiley, New Jersey, 2008), p. 97.
[19]F. Gori, G. Guattari, and C. Padovani, Opt. Commun. **64**, 491 (1987).
[20]V. Bagini, F. Frezza, M. Santarsiero, G. Schettini, and G. S. Spagnolo, J. Mod. Opt. **43**, 1155 (1996).
[21]M. Santarsiero, Opt. Commun. **132**, 1 (1996).
[22]C. F. R. Caron and R. M. Potvliege, J. Opt. Soc. Am. B **15**, 1096 (1998).
[23]Y. Li, H. Lee, and E. Wolf, J. Opt. Soc. Am. A **21**, 640 (2004).
[24]J. C. Gutiérrez-Vega and C. Lopez-Mariscal, J. Opt. A, Pure Appl. Opt. **10**, 015009 (2008).
[25]J. A. Stratton, *Electromagnetic Theory* (McGraw-Hill, New York, 1941), p. 1.
[26]J. Durnin, J. Opt. Soc. Am. A **4**, 651 (1987).
[27]J. Durnin, J. Miceli, and J. H. Eberly, Phys. Rev. Lett. **58**, 1499 (1987).
[28]W. G. Neubauer, R. H. Vogt, and L. R. Dragonette, J. Acoust. Soc. Am. **55**, 1123 (1974).
[29]L. R. Dragonette, R. H. Vogt, L. Flax, and W. G. Neubauer, J. Acoust. Soc. Am. **55**, 1130 (1974).
[30]See supplementary material at http://dx.doi.org/10.1063/1.3518496 for the animations related to the far-field acoustic scattering directivity patterns as well as the magnitude and phase distributions of the incident beam.
[31]F. G. Mitri, J. Phys. A: Math. Theor. **42**, 245202 (2009).
[32]F. G. Mitri, Eur. Phys. J. E **28**, 469 (2009).